# Dayside and nightside reconnection rates inferred from IMAGE FUV and Super Dual Auroral Radar Network data

B. Hubert,[1] S. E. Milan,[2] A. Grocott,[2] C. Blockx,[1] S. W. H. Cowley,[2] and J.-C. Gérard[1]

[1]   The spectrographic imager at 121.8 nm (SI12) of the far ultraviolet (FUV) experiment onboard the IMAGE spacecraft produces global images of the Doppler-shifted Lyman $\alpha$ emission of the proton aurora. This emission is solely due to proton precipitation and is not contaminated by dayglow, allowing us to monitor the auroral oval on the dayside as well as on the nightside. Remote sensing of the polar aurora can be advantageously supplemented by use of ground-based data from the Super Dual Auroral Radar Network (SuperDARN) that monitors the ionospheric convective flow pattern in the polar region. In the present study, the SI12 images are used to determine the location of the open/closed field line boundary and to monitor its movement. The SuperDARN data are then used to compute the ionospheric electric field at the location of the open/closed boundary. The total electric field is then computed along the boundary accounting for its movement via Faraday's law so that the dayside and nightside reconnection voltages can be derived. This procedure is applied to several substorm intervals observed simultaneously with IMAGE FUV and SuperDARN. The dayside reconnection voltage feeds the magnetosphere with open flux, which is later closed by nightside reconnection. The calculated dayside reconnection rate is consistent with the solar wind properties measured by the Geotail, Wind, and ACE satellites. We identify the presence of nightside reconnection due to pseudobreakups taking place during the growth phase. In several cases, we establish that the nightside reconnection rate is maximum at the time of the substorm expansion phase onset or shortly after, reaching $\sim$120 kV, and then slowly returns to undisturbed values of $\sim$30 kV. The flux closure rate can also start intensifying prior to expansion phase onset, producing pseudobreakups.

## 1. Introduction

[2]   In 1961, Dungey published a pioneering work sketching the general dynamics of the Earth's magnetic field line interaction with the solar wind [*Dungey*, 1961]. The "Dungey cycle" describes how field lines of the planetary magnetic field are opened at the dayside magnetopause by reconnection with the interplanetary magnetic field carried by the solar wind, are convected antisunward by the solar wind flow, then reconnect in the nightside tail thus returning to a closed topology, and are finally convected back to the dayside. The four steps of this cycle take place simultaneously in the magnetosphere almost all the time, creating the polar ionospheric convection. *Cowley and Lockwood*

[1992 and references therein] summarized how the sign of each IMF component influences the dayside reconnection and the convection flow pattern. In particular, significant magnetic flux opening is expected when the IMF $B_z$ component is southward (i.e., negative), but becomes greatly reduced when the IMF points northward.

[3]   The opening of magnetic flux at the dayside creates the necessary conditions to produce substorms via an accumulation of open magnetic flux and hence field energy in the magnetic tail. The period of time preceding a substorm expansion during which the magnetosphere "accumulates" open magnetic flux is often referred to as the growth phase. This phase is characterized by an increase in radius of the auroral oval. During subsequent substorm expansions, magnetic field lines that have previously been opened at the dayside and convected downtail by the solar wind reconnect within the tail plasma sheet, causing a substantial flux closure which releases accumulated field energy to the plasma particles. This reconfiguration of the tail magnetic field takes place together with poleward expanding auroral particle precipitation, and modification

---

[1]Laboratoire de Physique Atmosphérique et Planétaire, University of Liège, Liege, Belgium.
[2]Department of Physics and Astronomy, University of Leicester, Leicester, UK.

of the electric field, plasma flow, and currents flowing in the coupled magnetosphere-ionosphere system.

[4] Both dayside and nightside reconnection of field lines are associated with potential drops across the open/closed field line boundary, as can be understood by considering Faraday's law, as expressed in equation (1) [*Siscoe and Huang*, 1985; see also *Grocott et al.*, 2002; *Milan et al.*, 2003, 2004; *Milan*, 2004, and references therein]. Changes in the amount of open flux threading the polar cap $\Phi$ are related to the total electric field $\vec{E}$ by the expression

$$\frac{d\Phi}{dt} = -\oint_C \vec{E} \cdot \vec{dl}, \tag{1}$$

where C is the curve encircling the polar cap area S, and the open magnetic flux is

$$\Phi = \int_S \vec{B} \cdot \vec{n} \, ds, \tag{2}$$

$\vec{n}$ being the vector normal to the area S, and $\vec{B}$ the Earth's magnetic field. The electric field $\vec{E}$ must be computed in the frame of reference moving with the boundary C and is thus

$$\vec{E} = \vec{E}_i + \vec{v} \times \vec{B}, \tag{3}$$

where $\vec{E}_i$ is the ionospheric electric field measured in a frame of reference fixed with respect to the planet, and $\vec{v}$ is the velocity of the moving boundary C (normal to the boundary).

[5] Equation (1) relates to the rate of change of open flux in the system, equal to the difference between the rate of open flux production at the magnetopause and open flux closure in the tail. If these two rates are equal, for example, such that the amount of open flux is constant, then the line integral of the electric field around the boundary will be zero, as it is for any fixed closed contour containing a fixed amount of ionospheric magnetic field. When both the boundary motion and ionospheric flow (related to the electric field) are known, it is possible to obtain the rates of flux opening and flux closure separately. This can be done by integrating the electric field in the boundary frame around those segments of the boundary where flux is added to the open region, giving the "dayside" (or magneto-pause) reconnection rate, and where it is removed, giving the "nightside" (tail) reconnection rate. This is the task undertaken in this paper.

[6] The position of the polar cap boundary and its motion can be determined using spaceborne imaging instruments giving a global view of the auroral morphology, with the poleward limit of the auroral oval identified with the open/closed boundary. The ionospheric electric field can be determined from knowledge of the ionospheric con-vection flow pattern as determined, for instance, with the Super Dual Auroral Radar Network, using the method of *Ruohoniemi and Baker* [1998] to derive the electric field and potential across the whole polar cap. The flow velocity $\vec{v}_i$ and the ionospheric electric field are related to each other through

$$\vec{E}_i = -\vec{v}_i \times \vec{B}. \tag{4}$$

The convection flow pattern shows how newly opened field lines are introduced into the polar cap on the dayside, and are convected toward the nightside across the polar cap. It also shows how closed field lines are redistributed and convected back from the nightside to the dayside outside of the polar cap after nightside reconnection. In some circumstances, it is also possible to use the characteristics of the radar backscatter signal to infer the location of the open-closed field line boundary and to follow its motion [*Milan et al.*, 2003, and references therein]. However, the boundary position is not always unequivocal in such data, while generally the whole of the boundary is not observed because of limitations of radar coverage. *Chisham et al.* [2005] nevertheless showed from a statistical standpoint that the Spectral Width Boundary (SWB), the boundary between broad and narrow backscatter echoes, is a reliable proxy for the open/closed boundary close to noon and midnight. Note also that *Chisham et al.* [2004] measured the dayside reconnection rate during an interval of northward IMF combining SuperDARN and DMSP data.

[7] *Blanchard et al.* [1996, 1997a] developed a method to determine the local nightside reconnection rate using ground-based measurements of the emission of metastable oxygen O($^1$D) at 630 nm combined with radar measurement of the ionospheric flow, and applied it to the study of several substorms [*Blanchard et al.*, 1997b]. They found that the nightside reconnection rate increases shortly after substorm onset. This method however suffers from its spatial limita-tion, sometimes also introducing a time delay between the expansion phase onset and the measurement of the increase of the reconnection rate at some distance from the location of the onset. In addition, the auroral oxygen red line emission at 630 nm is strongly contaminated by the day-glow (the dissociative recombination of O$_2^+$ produces meta-stable oxygen), so that summer time studies are more difficult. This method is also generally inapplicable to the determination of the dayside reconnection rate due to this contamination, except perhaps in winter when the auroral oval is well separated from the dayside terminator.

[8] *Østgaard et al.* [2005] combined FUV images of the electron aurora with radar measurement from EISCAT to estimate the magnetotail reconnection rate, and found an event presenting a bursty reconnection electric field. These authors also summarized how the ionospheric electric field estimated along the open/closed boundary can be related to the field at the reconnection site, after the work of *Vasyliunas* [1984].

[9] In the present paper, we employ IMAGE FUV data to determine the morphology of the auroral oval and thus of the polar cap boundary on the global scale, combined with the ionospheric electric field deduced from the SuperDARN flow patterns, to compute the total open magnetic flux and the dayside and nightside reconnection rates. We propose a method capable of determining these quantities at any time of the year. The method is applied to study the temporal development of several substorms. Section 2 describes the method and data that are used. Section 3 discusses some uncertainties and tests the accuracy of our method in comparison with boundary identification using DMSP in situ particle measurements while section 4 presents the results obtained for several substorms. Section 5 then discusses the uncertainties of the method. The main results

are summarized in section 6. We show that the nightside flux closure is maximum at the time of substorm onset or shortly after, and that pseudobreakups taking place during the growth phase significantly increase the nightside closure voltage prior to onset.

## 2. Instrumentation and Analysis Techniques

[10] The IMAGE satellite was launched on 25 March 2000 into an eccentric orbit with an apogee of $\sim$7 $R_E$, a perigee of $\sim$1000 km, and an orbital period of $\sim$14 h. The FUV experiment [*Mende et al.*, 2000a, 2000b] includes three imagers of interest here, that generate an FUV image of the Earth every two minutes (the period of the rotation of the satellite on its axis). The Wide Band Imaging Camera (WIC) observes the $N_2$ LBH bands between 135 and 180 nm, the first channel of the spectrographic imager (SI13) is centered on the OI 135.6 nm transition, while the second channel of the spectrographic imager at 121.8 nm (SI12) observes the Doppler-shifted Lyman $\alpha$ emissions due to the proton aurora. The geocoronal Lyman $\alpha$ component at the rest wavelength 121.6 nm is efficiently rejected by the instrument, as well as the nearby NI 120 nm line. The WIC and SI13 cameras globally image emissions mostly produced by precipitating electrons. The additional contribution due to proton precipitation and the secondary electrons they generate can be obtained on the basis of the SI12 measurements. The snapshots taken simultaneously once every two minutes by the WIC, SI13, and SI12 imagers are well suited to a study of the dynamics, morphology and energetics of the global electron and proton precipitation.

[11] The data used to determine the polar cap boundary are the images of the proton aurora obtained with the IMAGE FUV SI12 imager. A threshold can be determined for each image individually on a statistical basis, to discriminate between the auroral signal and the image background. This threshold must be accurately determined, as the boundary sought corresponds to the limit where the auroral emission drops to zero. The SI12 images are preferred to SI13 and WIC, despite the higher sensitivity of the latter camera, and to a lesser extent the SI13 camera, since these cameras are more subject to dayglow contamination. This arises because the mechanisms producing the bulk of the auroral emissions and the dayglow emissions are similar. The Doppler-shifted Lyman $\alpha$ emission does not suffer from this drawback because these photons are emitted directly by the precipitating protons capturing an electron. SI12 images are never significantly contaminated by dayglow emissions and are thus well suited to a systematic determination of the auroral emission boundary. Indeed, in the present study, this issue is critical since the residual noise following dayglow subtraction must not be confused with the auroral signal, as we seek to identify the boundary of the auroral emission. However, for periods close to the winter solstice when dayglow is confined to lower latitudes near noon, the separation of the electron aurora from the dayglow is often unambiguous, especially when the polar cap is small, giving us the opportunity to compare the open flux determined with the SI12, SI13, and WIC imagers. In addition, *Sergeev et al.* [1983] showed that the chaotization of the velocity distribution of the trapped protons feeding the proton aurora is due to the violation of the first adiabatic invariant on the closed stretched field lines of the magnetotail. It is thus legitimate to consider that significant proton precipitation occurs along closed field lines. We can thus expect to use the poleward limit of the proton aurora to set up a reasonable proxy for the open/closed field line boundary. This is however a nontrivial problem subject to uncertainties, which is affected by sensitivity threshold issues.

[12] The Super Dual Auroral Radar Network (Super-DARN), also used in this study, collects data from nine radars in the northern hemisphere (eight radars during the period of interest). The radar pulses scatter from naturally occurring irregularities in the ionospheric plasma, the time delay between emission and echo giving the location of the scattering volume, and the Doppler shift of the echo giving the velocity of the plasma perpendicular to the field lines along the line of sight. *Ruohoniemi and Baker* [1998] developed the "map potential" method to reconstruct the ionospheric convection pattern and the associated electric field using the ensemble of line-of-sight velocity values available from all the SuperDARN radar operating during a particular interval. The electric potential is expressed as a series of spherical harmonics whose coefficients are determined using a least squares fit technique applied to the measured component of the flow velocity. A statistical model of the ionospheric convection flow is also used [*Ruohoniemi and Greenwald*, 1996], that accounts for the interplanetary properties when they are known, allowing to constrain the fitted potential over areas of the polar region where no data are available. The method is conceived such that as little information as necessary is introduced from the model to prevent the fitted potential from having an unrealistic behavior [*Ruohoniemi and Baker*, 1998]. As pointed out by *Grocott et al.* [2002] when data are missing over an active portion of the oval, during the expansion phase of a substorm for example, the fitted potential can be less reliable over that part of the oval, since the model used to constrain the least squares fit in that area represents an "averaged" situation rather than the specific conditions prevailing for a particular event, which may depart from the average in the active portion of the oval at that time. In the present study, we selected intervals with a good Super-DARN coverage to reduce the effect of potentially inaccurate input from the model used to constrain the "map potential" method in the uncovered areas.

[13] In the analysis presented here, the poleward boundary of the auroral oval is identified from the IMAGE FUV SI12 data as indicated above, fitted with a Fourier series, and its velocity determined from the displacement in successive images. The fitting of the boundary with a Fourier series is necessary to extrapolate the boundary in regions where the proton aurora is not bright enough to be detected with the SI12 instrument. A series of five harmonics is generally used. Using more harmonics in the series would increase the risk of having local artificial oscillations that would impair the quality of the physical results. In addition, the time derivative is very easy to compute numerically when it is expressed with a Fourier series, only the coefficients of the series being dependant on time. The total electric field in the frame of reference of the boundary can then be computed by combining these results with the electric field of the ionospheric flow from the SuperDARN

data. Faraday's law is then applied to compute the opening (dayside) and closing (nightside) potential drops, integrating the electric field across the moving boundary. Regions of positive (negative) $\vec{E} \cdot \vec{dl}$ were considered as threading the dayside (nightside, respectively) reconnection site. Note that the net contribution of the electric field associated with the ionospheric flow to the rate of change of the open magnetic flux is zero, since it represents the voltage across a closed static loop. Nevertheless, this electric field cannot be neglected when computing the nightside and dayside reconnection voltages separately.

[14] For validation purposes, we concentrate on a restricted set of data collected during the winter season in 2000 when an adequate coverage of the auroral region is guaranteed both for the IMAGE FUV and SuperDARN data. These time intervals contain at least one substorm whose onset has been observed in the IMAGE FUV data. Using these data, we then study both the period when the polar cap expands because of significant dayside reconnection and weak nightside reconnection, and the following period of intense flux closure on the nightside during substorms.

## 3. Reliability of the Boundary Determination

[15] As mentioned before, the advantage of using the SI12 images of the proton aurora to estimate the location of the open-closed field line boundary is the absence of dayglow contamination, so that global coverage can be achieved on the nightside and dayside at any time of the year, for any size of the auroral oval. It nevertheless suffers some limitation. Because of the sensitivity threshold, proton precipitation along the polewardmost field lines may be too weak to produce Lyman $\alpha$ emission detectable with SI12, biasing the location of the boundary equatorward. This would result in an overestimation of the open magnetic flux. As a side effect, when the oval suddenly brightens, areas previously threaded by closed field lines located poleward of the optical boundary may light up in the detector, resulting in an artificial poleward motion of the boundary. It is thus necessary to clarify the relation linking the optical SI12 poleward boundary and the open/closed field line boundary. As this source of error depends on the auroral brightness through the instrument detection threshold, it is natural to search for a correction that depends on the SI12 count rate.

[16] We compared the location of the SI12 poleward boundary with the location of the b5e, b5i and b6 boundaries determined with the DMSP in situ particle flux data. We also conducted a comparison with the open/closed field line boundary deduced from the classification of particle regimes using the DMSP in situ measurements (which we will note as "boc" when deduced from DMSP particle measurements) as described by *Newell et al.* [1991], and as was done by *Blanchard et al.* [1997a]. DMSP b5e and b5i correspond to the location where the flux and/or energy of electrons and protons, respectively, drop abruptly. Boundary b6 is the poleward limit of the auroral drizzle. The boc boundary is identified when a transition is observed in the origin of the precipitating particles from a known closed region to a known open region of the magnetosphere. The b5e and b5i limits are generally close to each other on the

spatial scale of interest in the present problem (the size of an SI12 pixel projected on the planet surface is roughly 1° MLAT). Although weak proton precipitation can be measured in the drizzle between the b6 boundary and the polewardmost b5 boundary, this does not guarantee that all these field lines are closed (P. T. Newell, personal communication, 2005). For completeness, we conducted a statistical study comparing the location of the b5e, b5i and b6 boundaries with the open/closed field line boundary inferred from the systematic dayside classification of polar regions based on the DMSP particles measurements, that is, boc [*Newell et al.*,1991]. The difference between the magnetic latitude of the boc boundary and of the b5i (b5e, b6) boundary is on average 1.45° ± 0.055° (1.22° ± 0.058°, −1.15° ± 0.057°, respectively), the standard deviation of this difference being 2.75° (3.17°, 2.81°, respectively). We also compared the average value ($MLAT_{b5i}$ + $MLAT_{b6}$)/2 with the latitude of the DMSP boc boundary and found that the difference between these two is on average 0.02° ± 0.069°, with a standard deviation of 2.45°. We conclude that the open/closed field line boundary deduced from the DMSP classification lies midway between the b5i and b6 boundaries on average. Both the b5i and b5e boundaries are a little more than a degree equatorward of the boc boundary, while the b6 boundary is 1.15° poleward of the boc. This value can be compared with the spatial resolution of spaceborne global imagers. In a previous study, *Baker et al.* [2000] compared the latitude of the b5e boundary with Polar UVI data, and found the b5e boundary lies 1° poleward of the optical boundary determined by Polar UVI. Our study thus suggests that the boc boundary lies on the order of ∼2.5° poleward of the Polar UVI boundary, on average. Note also that *Blanchard et al.* [1995, 1997a] used the DMSP classification to calibrate their method of determination of the open-closed boundary on the basis of the metastable O($^1$D) emission at nighttime, and estimated an accuracy of 0.9° invariant latitude.

[17] Our study compares the optical boundary of the proton aurora as seen with IMAGE FUV SI12 with the DMSP boundaries. Figure 1 summarizes our comparison between the DMSP boundary locations and the optical boundary of the proton aurora. We compare the SI12 proton optical boundary and the b5e (not shown), b5i, b6 and boc boundaries. Let r be the sine of the colatitude of the boundary, that is, the radius of the boundary projected in the equatorial plane. We fitted a decreasing exponential function on the relative difference ($r_{SI12}$ − $r_{DMSP}$)/$r_{SI12}$ as a function of the maximum SI12 count measured in a 1h MLT sector centered on the location of the DMSP boundary. Despite some scatter, the bulk of the data show that when the aurora is bright, the SI12 and DMSP b5e, b5i and b6 boundaries match each other fairly well. At lower count rates, a correction should be applied, on the basis of the exponential function fitted to the data, representing the average discrepancy between the optical boundary of the proton aurora and the DMSP b5i and b6 boundaries. Surprisingly, no such relation could be established between the maximum count rate and the difference of the boc and SI12 boundary locations. Instead, we found that the boc boundary lies on average 0.55° ± 0.093° poleward of the SI12 boundary (standard deviation: 2.76°).
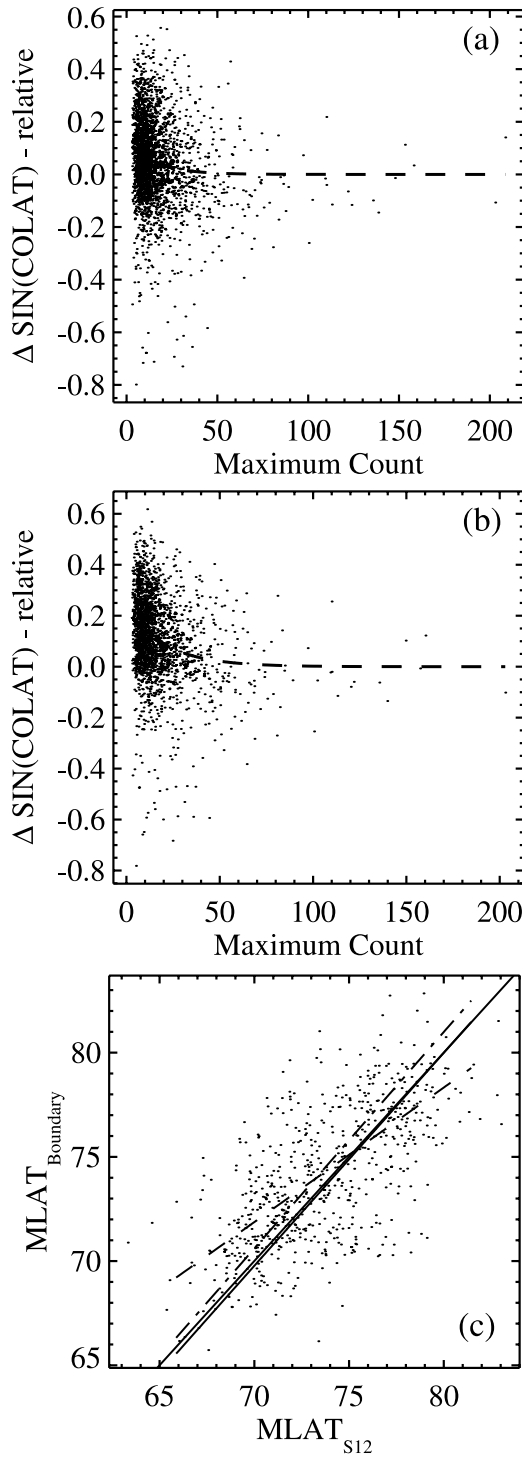
**Figure 1.** Relative difference of the sine of the colatitude of the DMSP boundary and the SI12 optical boundary as a function of the maximum SI12 count measured in the MLT sector of the DMSP satellite pass for DMSP boundaries (a) b5i and (b) b6 with a fitted exponential function. (c) Magnetic latitude of DMSP boc boundary as a function of the SI12 optical poleward boundary. The solid line is the bisector, the dashed line is the regression curve, the dash-dotted line results from a least squares fit through the data, and the dash-triple-dotted line results from a minimax fit.

It must be noted that the boc boundary location differs in nature from the b5e, b5i and b6 boundaries. While the b5e, b5i and b6 boundaries rely on quantitative variations of the precipitating flux, the boc boundary relies on the properties of the spectrum of the precipitating particles, allowing their magnetospheric origin to be identified. It is thus intuitively natural that the SI12 boundary relates to the b5 and b6 boundaries through the quantitative properties of the aurora, whereas the relation with the boc location does not necessarily need to. Note in addition that the regression line fitted to the data in Figure 1c (dashed line) does not match the bisector (solid line), but a best line minimizing the maximum distance between the data and the fitted line (dash-triple-dotted line) is very close to the bisector, whereas the best line minimizing this distance in a least squares sense (dash-dotted line) is roughly parallel to the bisector at a distance roughly reflecting the average difference between both variables. We thus correct the location of the SI12 boundary by a fixed amount of $\sim 0.55°$ and retrieve a more reliable estimate of the location of the open-closed field line boundary, in an average sense. Note that the geometry of the DMSP orbit is such that most of the data were acquired in the 18–24 MLT sector, and care should be taken in extrapolating the result to other MLT sectors. Nevertheless, there is no obvious reason to believe that the relation between boundary locations should be dramatically different in the 0–6 MLT sector, considering that this difference essentially relies on sensitivity limitations. The situation may be more critical around the noon sector, which has the additional complication that the cusp region is generally bright in the SI12 images, although it is threaded by open field lines. Consequently, we do not apply any correction in a 1 hour MLT sector centered on the noon sector, in an attempt to avoid worsening this bias.

[18] One drawback of using auroral data to identify the OCB is that while most aurora appear on closed field lines it is well known that the cusp aurora are on open field lines, so our technique underestimates the amount of open flux in the polar cap. However, we will now discuss why we feel that this introduces only a minimal error to the deduced reconnection rates. It is easily shown that, providing the orientation of the tangential (with respect to the boundary) component of the ionospheric electric field only varies slightly versus latitude on the scale of a few degrees, the shape of the moving boundary in the cusp region is not crucial for the computation of its contribution to the reconnection rate. Assuming that the sign of $\vec{E} \cdot \vec{t}$ (with $\vec{t}$ the unit vector tangent to the boundary) does not change along paths $\gamma_1$ and $\gamma_2$ described in Figure 2, the voltage between points A and B does not depend on the path chosen to integrate $\vec{E} \cdot \vec{t}$, so that the net voltage can be computed integrating along any path. If no significant flux closure takes place along field lines threading the noon sector, the contribution of the ionospheric electric field to the flux opening rate is reliably computed independent of the detail of the integration path in the noon sector. Considering now the motion of the boundary, the electric field responsible for the reconnection rate is the second term on the right-hand side of equation 3. Considering the open-closed boundary moves equatorward at velocity $v$
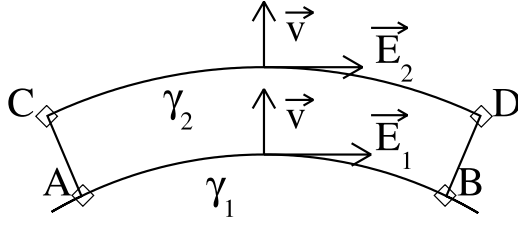
**Figure 2.** Sketch of two different approximations of the shape of the open/closed field line boundary in the cusp sector. Curve $\gamma_1$ is a circular arc between points A and B, while curve $\gamma_2$ starts at point A and follows a meridian to point C, then a parallel to point D and another meridian to point B. It is assumed that the boundary moves equatorward at velocity $v$ so that the motional electric field $E_{1(2)}$ associated with the motion of arcs $\gamma_{1(2)}$ is tangent to the parallel arcs (and perpendicular to any meridian arc).

(Figure 2), one can compute the motional voltage between points A and B along paths $\gamma_1$ and $\gamma_2$. Assuming a dipole field of magnetic moment $M$, and noting the colatitude $\lambda$, the magnetic permeability $\mu_0$ and the planet radius (at ionospheric altitude) $R$, the magnitude of the electric field is

$$E = \frac{\mu_0 M}{2\pi R^3} v \sin(\lambda), \tag{5}$$

and the motional voltages $V_1$ and $V_2$ between A and B (separated by an angle $\Delta\varphi$) along paths $\gamma_1$ and $\gamma_2$ respectively are

$$\begin{aligned} V_1 &= \Delta\varphi \frac{\mu_0 M}{2\pi R^2} v \sin^2(\lambda) \\ V_2 &= \Delta\varphi \frac{\mu_0 M}{2\pi R^2} v \sin^2(\lambda + \delta\lambda), \end{aligned} \tag{6}$$

assuming that both paths are $\delta\lambda$ apart in colatitude, so that the relative difference $(V_2 - V_1)/V_1$ is $(\sin^2(\lambda + \delta\lambda) - \sin^2(\lambda))/\sin^2(\lambda)$. At 70° MLAT, $\lambda = 20°$ and a difference $\delta\lambda = 1°$ in colatitude translates to a relative difference of $\sim$10% in the motional voltage computed between points A and B (in other words, $\frac{1}{V}\frac{\partial V}{\partial\lambda}\delta\lambda = 2\cot g(\lambda)\delta\lambda \approx 0.096$). At higher latitude, that is, at MLAT = 80°, the error computed in the same way is $\sim$20%. The impact on the total flux opening voltage computed in the cusp sector will depend on the relative contribution of the convection and motional electric fields to the potential drop. As the convection velocity is generally larger than the velocity of the motion of the boundary in the cusp sector, we can estimate a typical value of the relative error made on the flux opening voltage computed in the cusp sector by neglecting the detailed shape of the cusp when the ionospheric and motional voltages are equal: it ranges from $\sim$5% at 70° MLAT to $\sim$10% at 80° MLAT. Smaller errors will be made when the convection velocity is larger than the boundary motion velocity. Larger errors may however occur when the convection is weak and the motion of the boundary is large. The maximum relative error is obtained assuming that the ionospheric electric field is zero (i.e., only the motional electric field contributes to the reconnection voltage) and ranges from 10% at 70° MLAT to 20% at 80° MLAT, as computed

before. As already stated above, these errors refer to the systematic bias inherent to the mislocation of the open/closed field line boundary in the cusp sector only.

## 4. Case Studies

### 4.1. Case on 26 December 2000

[19] We first study the interval starting at 1715 UT on 26 December 2000 and ending at 0244 UT on 27 December 2000. During this 9 h 30 min period, the SI12 instrument made continuous observations of the northern polar region. Simultaneously, the SuperDARN radar network obtained measurements of the ionospheric convection pattern, so that the ionospheric electric potential and electric field can be retrieved. In addition, the Geotail satellite was ideally positioned to measure the solar wind properties upstream of the Earth's magnetosphere. Figure 3 presents a set of IMAGE SI12 snapshots obtained during the interval, shown in a polar projection. This interval was preceded by a very long (more than 12 hours) period of negative IMF $B_y$, displacing the northern auroral oval to the dusk side by an exceptionally large shift. The fitted polar cap boundary is overlaid as the continuous white line. This fitted boundary does not strictly follow the image boundary, as it results from a least squares fit, but it nevertheless gives a very
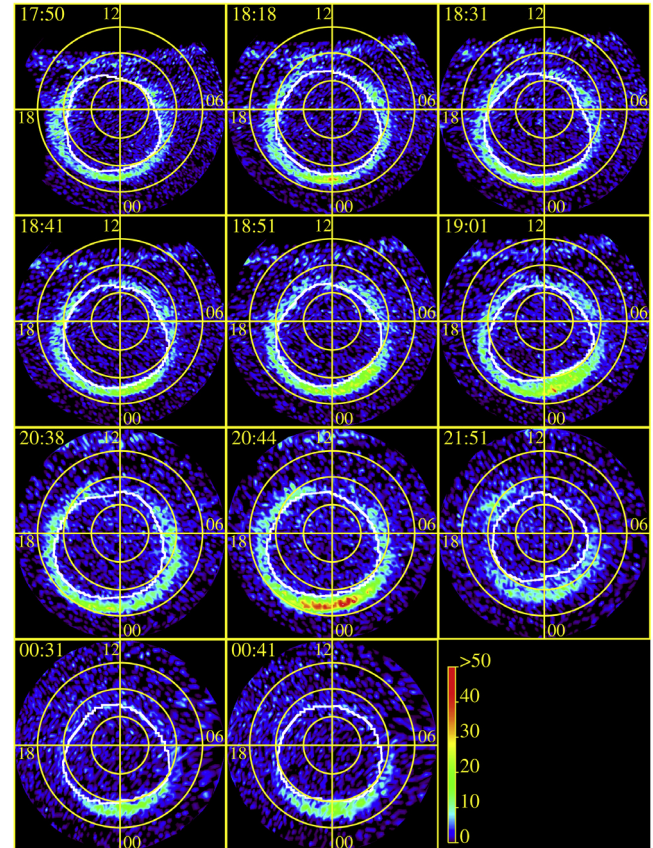


**Figure 3.** Sample of polar views of the proton aurora obtained with IMAGE FUV SI12 obtained between 1710 UT on 26 December 2000 and 0200 UT on 27 December 2000. The fitted open/closed field line boundary is overlaid in white. The color scale is expressed in SI12 counts.
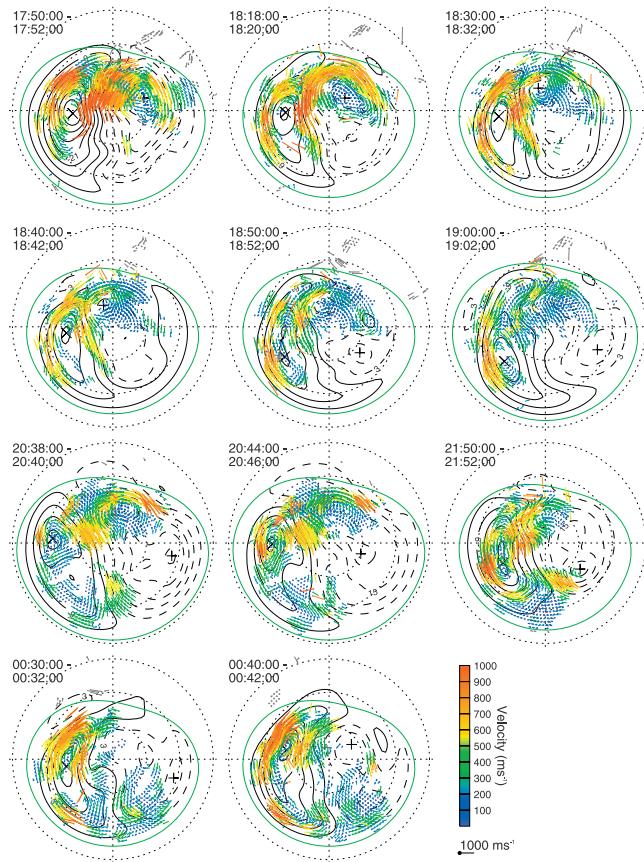
**Figure 4.** Sample of polar views of the convection flow deduced from SuperDARN measurements obtained between 1710 UT on 26 December 2000 and 0200 UT on 27 December 2000, showing equipotentials of the electric field associated with the flow. Data were accumulated for 2 min in each plot.

good overall representation of the boundary. The simultaneous flow and electric potential patterns obtained with the SuperDARN network (data accumulated over 2 min intervals) are presented in Figure 4. Velocity vectors are reconstructed consistently with the fitted electric potential. The coverage of the polar region is incomplete because of the absence of radar coverage in the Siberian sector of the polar region, so that the electric potential pattern is completed using the technique of *Ruohoniemi and Baker* [1998]. Figure 5 also shows the solar wind properties as measured by the Geotail satellite during the period of interest. The satellite crossed the bow shock after 0130 UT, and those data should be used with care.

[20] The open magnetic flux Φ was computed for each SI12 image obtained during the interval. Its time derivative can then be computed directly following appropriate smoothing of the curve. The smoothing is realized using a series of boxcar average smoothings of decreasing width. Investigation showed that this method produces results similar to Gaussian smoothing and to digital filtering. The advantage of our method is that it rigorously conserves both the low-frequency shape and the integral of the smoothed function, which may not be the case with the other methods when applied to an interval of finite size. Both the computed magnetic flux and its derivative are shown in Figure 6. The
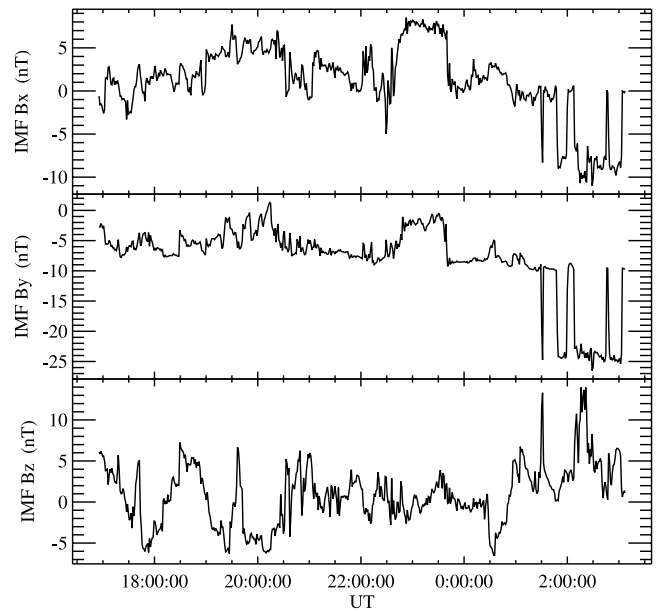


**Figure 5.** IMF (GSM) components from Geotail spacecraft measurements on 26 and 27 December 2000. After 0130 UT on 27 December, the satellite entered the magnetosheath. Data after this time thus no longer directly represent interplanetary conditions.
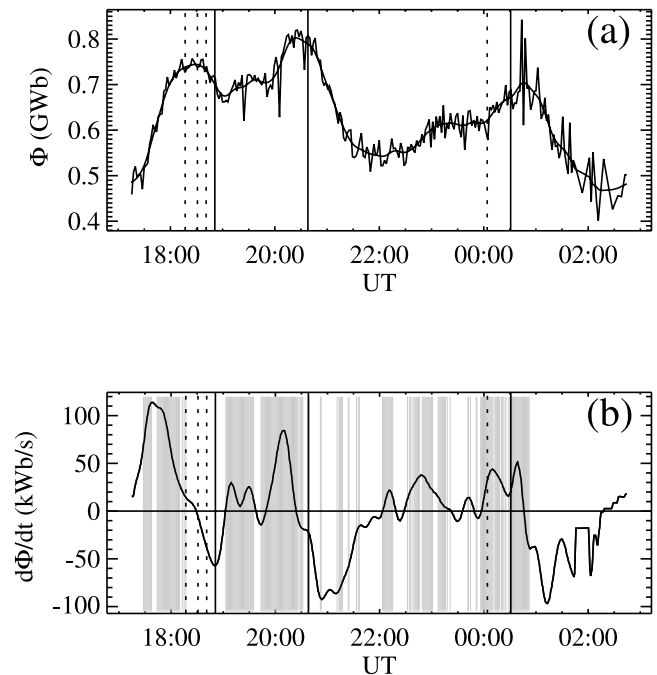


**Figure 6.** (a) Open magnetic flux (raw and smoothed values) threading the northern polar cap versus universal time, as deduced from SI12 data on 26 and 27 December 2000. (b) Time derivative of the smoothed open magnetic flux shown in Figure 6a. Shaded areas indicate periods of southward IMF from the Geotail data shown in Figure 5 (which are not relevant after 0130 UT). Vertical solid lines indicate the times of substorm onsets, while dashed lines indicate pseudobreakups.

noisy variations about the smoothed curve a give an idea of the reliability of the method; uncertainties appear to be lower than ∼10%.

[21] We verified that the open flux value deduced from the SI12 images is often smaller than that deduced from the SI13 images (not shown). This indicates that our estimate of the auroral limit using SI12 data is more accurate, since less equivocal identification of where the auroral signal drops to zero is expected usually to lead to smaller open flux estimates. We also verified that the open flux values deduced from the WIC images (not shown) often agree well with the SI12 values, except for some periods where these values significantly depart from each other, the value deduced from WIC being generally the larger. The quality of the Φ values deduced from WIC images strongly decreases (sometimes giving unrealistic values) when the auroral oval is weak on the dayside, such that the inferred boundary expands and approaches the terminator. This tends to indicate that the Φ values deduced from SI12 images are the most reliable, even during winter time. We attribute this higher reliability not to higher sensitivity, but rather to the fact that the SI12 images can be more simply analyzed and interpreted.

[22] Returning to Figure 6, we note that the shaded intervals in Figure 6b correspond to intervals of southward IMF, that is, to intervals where significant dayside reconnection rate can be expected, although moderate dayside reconnection can also occur during intervals of positive IMF $B_z$, especially when appreciable IMF $B_y$ is also present. These southward IMF intervals are seen to match periods of positive derivative of Φ, unless significant nightside reconnection also takes place. Pseudobreakups and substorm onsets can easily be identified using the FUV imagers [*Gérard et al.*, 2004], especially the WIC and SI13 instruments. Substorm onsets and pseudobreakups often appear less clearly in the SI12 images. The accuracy of the timing of the identified features is of course limited by the time resolution of the FUV images, that is, 2 min. Pseudobreakups are identified as a brightening initiated in a localized portion of the auroral oval, similar to an expansion phase onset, but that does not evolve into an expansion phase. They differ from poleward boundary intensifications (PBIs), such as those presented in Figure 2 of *Lyons et al.* [2002], both in location and morphology. At the start of the interval, Φ increases until ∼1817 UT, when a first pseudobreakup takes place, followed by two other pseudobreakups at 1831 and 1841, and a weak substorm onset at 1851 UT. The times of the pseudobreakups are indicated in Figure 6b by the vertical dashed lines, while the substorm onsets are shown by the vertical solid lines. Note also that the SI12 images and SuperDARN data obtained at times discussed in this paragraph are shown in Figures 3 and 4. The onset develops into a short-lived substorm-like event fading after ∼1915 UT. Φ then increases again until ∼2038 UT, when a further substorm onset takes place, resulting in enhanced auroral FUV emission. The substorm auroral brightness progressively fades after 2150 UT, and Φ starts increasing once more until ∼0031 UT (27 December 2000) when a third substorm onset is observed, followed by bright auroral emission and nightside flux closure.

[23] Throughout this interval, SuperDARN data coverage was sufficient to allow reliable measurement of the iono-
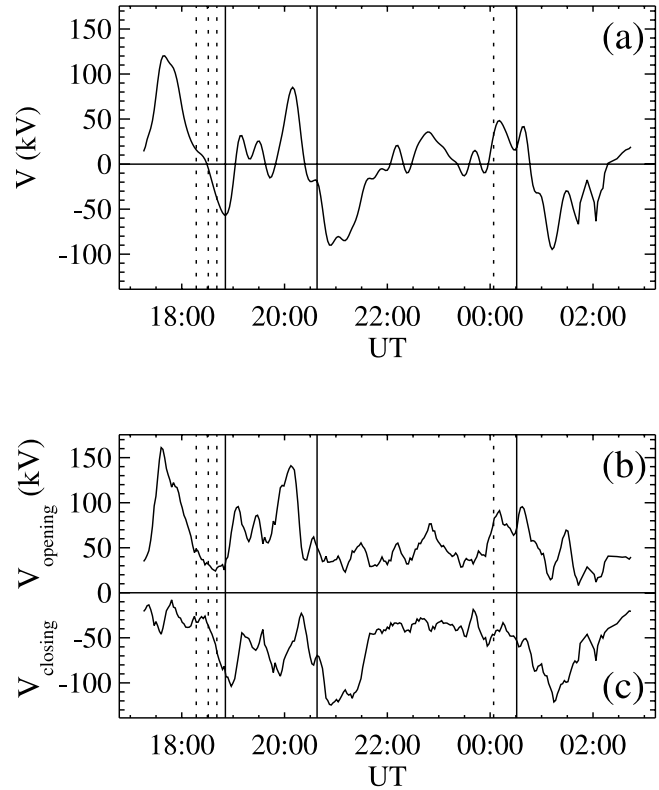


**Figure 7.** (a) Difference between dayside and nightside reconnection voltages for the interval on 26–27 December 2000, equal to the rate of change of open flux; (b) dayside reconnection voltage (i.e., open flux production rate); and (c) nightside reconnection voltage (i.e., open flux closure rate), obtained using the boundary motion deduced from SI12 images and the convection electric field deduced from SuperDARN data. As in Figure 6, vertical solid lines indicate the times of substorm onsets, while dashed lines indicate pseudobreakups.

spheric velocity over an extended area of the northern polar region, from which the associated electric field and potential can be determined. The dayside and nightside reconnection rates were then calculated using the method described above in sections 1 and 2. These are presented in Figure 7, together with their net value (i.e., the total rate of change of open flux). Note that the net reconnection rate computed by applying Faraday's law and by deriving Φ versus time (shown in Figure 6b) are identical, as expected from Maxwell's equations, so that internal consistency is guaranteed despite the potential sources of numerical errors. Also, the calculated nightside and day-side reconnection rates associated with the flow itself actually cancel each other as expected, since their sum represents the potential drop across a static closed loop. The period of rapid growth of Φ between 1730 and 1815 UT (see Figure 6) is characterized by intense dayside convection flow into the polar cap with flow speeds sometimes exceeding 1000 m s$^{-1}$ locally, indicating that dayside reconnection is feeding the polar cap with open flux. The nightside "return" flow speeds range between ∼300 and ∼650 m s$^{-1}$ with a few local excursions above 700 m s$^{-1}$. This relatively high return flow speed is due to an expan-

sion of the region of open flux into the nightside, rather than to an increase in the nightside reconnection rate, as is shown in Figure 6 and also in Figure 7. The period of time rich in pseudobreakups extending between ~1815 and ~1850 UT has dayside convection velocities peaking at ~800 m s$^{-1}$ at 1820 UT, then falling to ~600 m s$^{-1}$ at 1850 UT in the center of the polar cap, and with variable nightside return convection velocities reaching ~600 m s$^{-1}$, as directly measured in the dawn sector, related to episodes of flux closure in the nightside magnetosphere. The size of the polar cap was nonincreasing during that time interval, as can be seen in Figure 6. The following interval sees the open flux increasing again, with significant dayside convection driving newly opened field lines into the polar cap at speeds up to ~600 m s$^{-1}$. The open flux increases more steeply after ~1950 UT, indicating intense dayside reconnection (see Figure 7). After the substorm onset taking place at 2038 UT, the nightside return convection flow remains moderate, with the open/closed field line boundary retracting poleward because of nightside reconnection, reaching a tail reconnection voltage of 130 kV at ~2050 UT. After ~2200 UT, Φ increases slowly because of the effect of moderate dayside reconnection (between 30 and 90 kV) opening magnetic flux, in the presence of small nightside reconnection (~30 kV) closing only a small amount of magnetic flux. The convection flow measured in the dusk sector increases as the polar cap expands, and reaches velocities larger than 1000 m s$^{-1}$ for an extended period of time. The substorm observed by IMAGE FUV with an onset at 0031 UT on 27 December, is characterized by a nondecreasing Φ during its first stage of development, due to the competing effect of dayside and nightside reconnection, so that the return flow velocity driven by the nightside flux closure remains high at values larger than 1000 m s$^{-1}$ until 0110 UT. After that time, the polar cap starts shrinking rapidly and the flow velocity drops to values of ~600 m s$^{-1}$.

[24] The nightside reconnection rate in Figure 7 is more intense during the auroral substorm expansion phases. Note that a maximum of flux closure rate appears as a valley in our plots. The computed closure rate increases rapidly around the time of the onset, as expected, but the steep increase in magnitude of the nightside closure voltage starts about 18 (16) min prior to expansion phase onset at 2038 (0031) UT. However, in order to reliably compute the velocity of the boundary, some temporal smoothing had to be applied, as indicated above. Consequently, our method is not able to correctly represent large potential variations taking place on a very small timescale. We test this numerical limitation in Figure 8, applying our smoothing method to a simulated signal reproducing the closure voltage of a possible idealized onset (Figure 8a) and of the same curve preceded by a possible idealized pseudobreakup (Figure 8b). We assume that the onset develops in ~6 min reaching ~125 kV, after which the voltage then declines at a rate of 2 kV per minute (a reasonable value considering the actual cases) until it returns to the value it had prior to onset. The smearing due to the smoothing procedure results in an error of ~12 min in the start of the negative voltage increase. The minimum voltage (i.e., the maximum magnitude of the reconnection rate) is then reached ~6 min after the extremum of the actual signal,
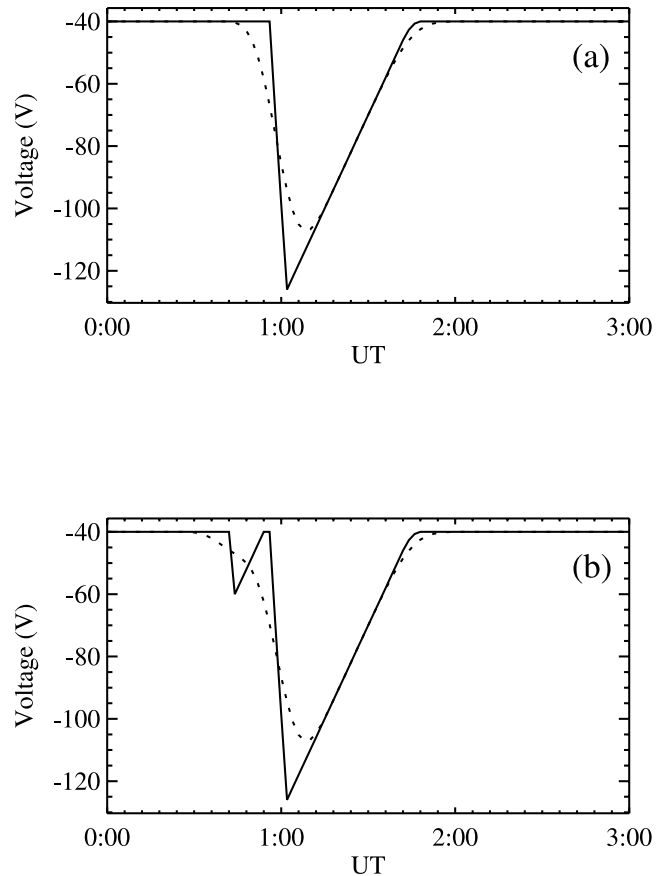


**Figure 8.** Simulated rapidly varying potential (solid curve) and its smoothed counterpart (dashed curve): (a) smoothed curve starts decreasing ~12 min before the solid curve and reaches its minimum ~6 min later, and (b) disturbance added prior to the main variation results in a broader smoothed curve that does not exhibit two extrema.

and its value is about 15% smaller in absolute value. A time resolution of two minutes was used in this simulation, equal to the time resolution of our data sets. Consequently, when studying rapidly varying potentials, delays of less than ~16 min are not significant, and the computed voltages will exhibit variations earlier than actually took place. Note as well that a possible pseudobreakup taking place prior to the onset would not be explicitly resolved (panel b), so we cannot determine the detailed time variation of the closure voltage. We conclude that the intensification of the flux closure takes place roughly at the time of the substorm expansion onset, identified at 2038 UT using the IMAGE FUV images. The maximum closure voltage obtained during the 2038 UT substorm is ~120 kV, but could be as high as ~140 kV, accounting for the bias induced by the smoothing. The maximum is reached at or shortly after substorm onset. The substorm-like event observed starting at 1851 UT was preceded by a series of pseudobreakups, and the computed nightside voltage intensifies 24 min prior to the breakup at 1851 UT. We conclude that flux closure took place significantly prior to the 1851 UT onset, resulting in the series of pseudobreakups, consistently with the results of *Aikio et al.* [1999]. Our method does not allow us to discriminate between a sudden

transient increase of the flux closure at the time of the pseudobreakups and a progressive increase ending in the onset. The nightside reconnection rate reaches its maximum magnitude (~100 kV) roughly at the time of onset of this event or shortly after, and could be as high as ~120 kV accounting for the applied smoothing. The substorm starting at 0031 UT (27 December) was preceded by a moderate pseudobreakup at 0004 UT, but no significant intensification in the magnitude of the nightside reconnection rate is indicated between these two events. Nor in this case does the potential drop reach its maximum magnitude around the time of onset, but rather at 0115 UT. The IMAGE FUV images show that several local bright spots appeared during the development of this substorm, suggesting that the mechanism governing its evolution might be more complex than for the other two events discussed above. In Figure 7c, the 0031 UT onset nevertheless appears to be associated with a local extremum of the nightside reconnection rate. The calculated maximum nightside reconnection rate is 116 kV at 0115 UT (possibly as high as ~130 kV for reasons discussed above).

[25] The dayside reconnection rate is often estimated using a transfer function based on upstream interplanetary properties. One example of a widely used function is given by

$$F = v_{SW} \ B_T \ sin^4\left(\frac{\theta}{2}\right),\qquad(7)$$

where $v_{SW}$ is the solar wind velocity, $B_T$ is the strength of the transverse IMF, and $\theta$ is the IMF clock angle with respect to north [*Wygant et al.*, 1983; *Liou et al.*, 1998]. This transfer function has the dimension of an electric field and must thus be multiplied by a characteristic length in order to retrieve a voltage. For southward IMF ($\theta = 180°$), this characteristic length L represents the width of the solar wind channel, transverse to the field, which reconnects with the terrestrial field at the magnetopause. Two approaches can then be proposed. As a first-order approximation (method 1) one can deduce L from the transfer function computed using the solar wind properties and the open flux determined, for example, from global imaging of the polar region (i.e., using IMAGE FUV SI12 images) during periods of time when the nightside reconnection rate is expected to be negligible [*Milan et al.*, 2003, 2004; *Milan*, 2004]. We can further refine this approximation (method 2) and compute the ratio between the dayside reconnection rate of Figure 7b and the transfer function of equation 7. The ratio of the dayside reconnection rate (Figures 7b and 9b) and the computed transfer function (Figure 9a) is shown in Figure 9c. Reasonable values of the characteristic length are obtained when both the transfer function and the dayside voltage are sufficiently large, giving L ranging between 4 and 15 $R_E$. The characteristic length deduced using the first method is 11 $R_E$ for the first substorm of the interval (with onset at 1816 UT), compared with ~10 $R_E$ obtained at 1800 UT in Figure 9b, and ~3 $R_E$ for the second and third (with onsets at 2038 and 0031 UT), compared with ~10 $R_E$ at 2000 UT and ~6 $R_E$ at 0030 UT. Both methods give results which are not, in essence, different from each other, giving L values of a similar order of magnitude, but method 1 is dependent on the reliability of the assumption of negligible nightside
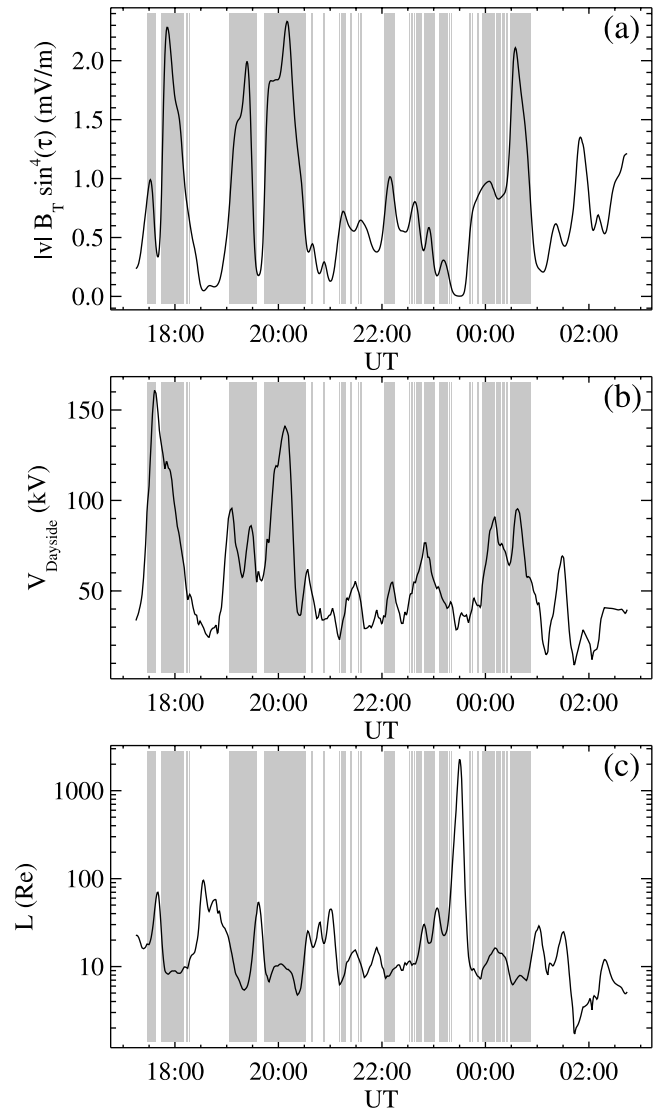


**Figure 9.** (a) Transfer function given by equation (7) calculated from the Geotail solar wind data on 26 and 27 December 2000 (irrelevant after 0130 UT), (b) dayside reconnection rate computed using SI12 and SuperDARN data, and (c) solar wind reconnection scale width L calculated from the ratio of Figures 9a and 9b. Shaded areas indicate intervals of southward IMF.

reconnection. This can be critical as we have seen in the present case that the nightside reconnection rate can increase prior to substorm onset, and is generally not less (in absolute value) than ~30 kV.

[26] As mentioned in the preceding paragraph, we find that tail reconnection closes magnetic flux at all times, with a typical voltage of ~30 kV during quiet periods. The location of the reconnection site still has to be identified. The quiet time closure voltage is fairly stable, while the voltage of substorm expansion phases exhibits a strong temporal dependence, and during the recovery phase, it progressively returns to a voltage similar to the value prevailing prior to onset. This suggests that the quiet time reconnection rate has not been dramatically modified by the explosive flux closure of the expansion phase. We speculate
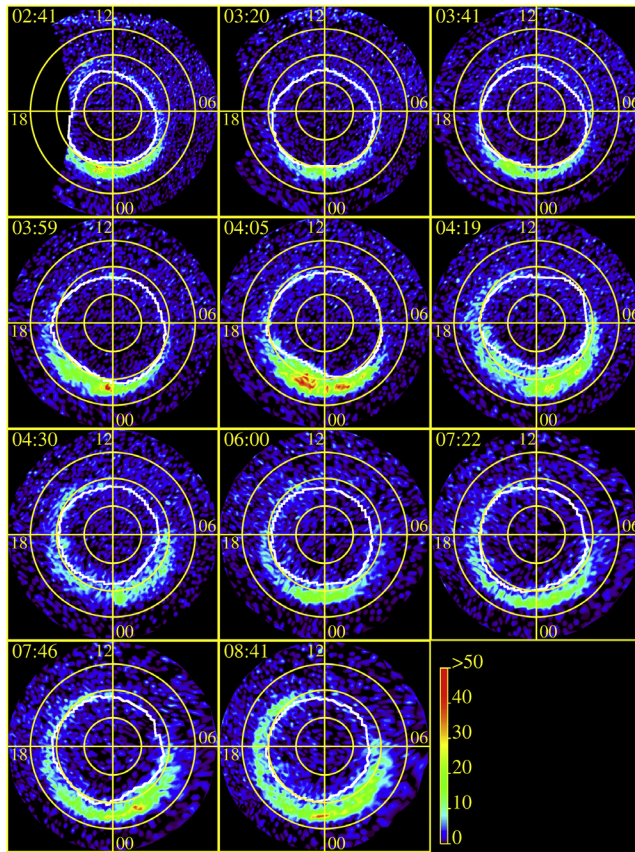
**Figure 10.** Sample of polar views of the proton aurora obtained with IMAGE FUV SI12 between 0235 and 1120 UT on 29 December 2000. The fitted open/closed field line boundary is overlaid in white. The color scale is expressed in SI12 counts.

that this quiet time flux closure takes place in the more distant magnetotail, in accordance, for example, with ISEE 3 measurements [*Feldman et al.*, 1984, 1987; *Smith et al.*, 1984; *Ho et al.*, 1994].

### 4.2. Case on 29 December 2000

[27] The IMAGE FUV instruments also provided continuous coverage of the northern auroral FUV emissions between 0215 and 1045 UT on 29 December 2000. A sample of SI12 images corresponding to this interval is presented in a polar view in Figure 10. The corresponding convection velocity and electric equipotentials deduced from the SuperDARN data are presented in Figure 11. A first pseudobreakup is seen at 0241 UT. Two other pseudobreakups occurred at 0320 and 0341 UT, followed by a substorm onset at 0359 UT. A quieter period followed this substorm with variable activity, especially along the polar boundary of the electron aurora, which showed what we identify as a poleward boundary intensification (PBI), similar with those shown by *Lyons et al.* [2002]. The opened magnetic flux and its time derivative were computed for this interval using the IMAGE FUV SI12 images of the proton aurora and are shown in Figure 12. The shaded regions of Figure 12b indicate southward IMF as observed by the Wind satellite (Figure 13) (the Geotail satellite was not favorably positioned at this time). During this interval

Wind was located at GSE $(X, Y, Z) \approx (6, 250, -17)$ $R_E$, such that an IMF propagation time to Earth of only ~1.5 min has been allowed for (an additional small time delay is also added for propagation through the magnetosheath and inner magnetosphere to match the auroral signature). Measurements from both the ACE and Wind satellites indicate a continuous period of southward IMF. Only one transient northward excursion is present in the Wind data (and absent in the ACE data) around 0335 UT. As expected for such IMF conditions, the open magnetic flux generally increases in time, except during the substorm expansion phase, and after 0700 UT, apparently due to an intensification of the auroral activity of the PBI. In addition, no trigger based on an IMF $B_z$ sign reversal can be associated with the substorm development, nor can a growth phase period be defined on the basis of IMF $B_z$ reversals. Nevertheless, this period presents an interval of open flux growth followed by an expansion onset that will be discussed in the next paragraphs.

[28] The SuperDARN radar network offered very good coverage of the northern polar region during the interval from 0200 to 0450 UT (Figure 11). Later, fewer data are available, but the electric field and potential can still be retrieved. As in the previous example, we thus computed the net rate of change of the amount of open flux as well as the
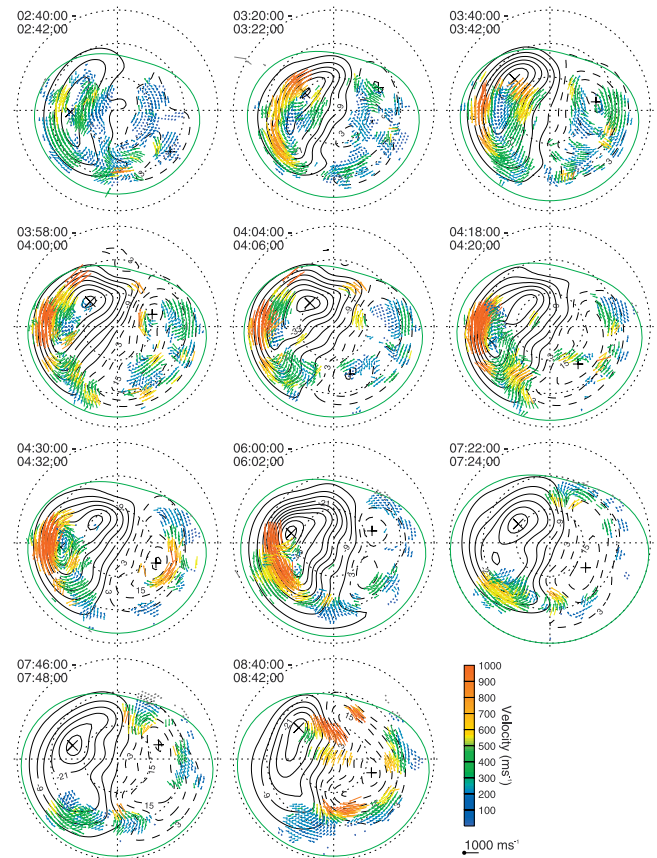


**Figure 11.** Sample of polar views of the convection flow deduced from SuperDARN measurements obtained between 0235 and 1120 UT on 29 December 2000, showing equipotentials of the fitted electric field. Data were accumulated over 2 min in each plot.
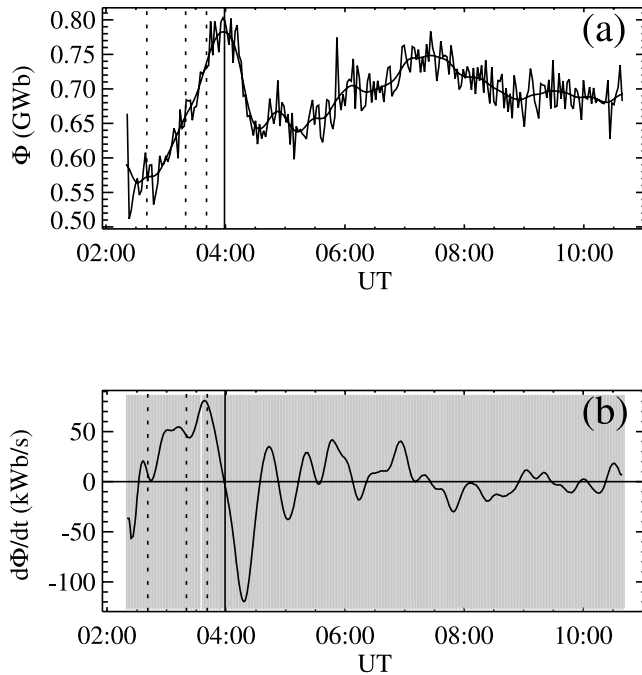
individual "dayside" and "nightside" reconnection rates using both the SuperDARN and IMAGE FUV SI12 data (Figure 14). Again, the voltage along the moving boundary computed by applying Faraday's law (Figure 14a) and deriving the open flux versus time (Figure 12b) are identical, as expected, so that internal consistency is guaranteed. As in the preceding case, the measured return flow speed was often high during time intervals of increasing $\Phi$, occasionally reaching 800 m s$^{-1}$. After the substorm onset at 0359 UT the return flow remained high, reaching 1000 m s$^{-1}$, despite the decreasing size of the polar cap. After ~0430 UT, the substorm intensity weakened and the competition between nightside and dayside reconnection leads overall to a slowly increasing amount of open magnetic flux. The steep increase of open flux taking place around 0600 UT is characterized locally by a high return flow velocity (more than 1000 m s$^{-1}$).

[29] During and preceding the substorm, the computed nightside voltage shown in Figure 14c has a temporal dependence similar in shape to that computed for 27– 28 December. Again, the nightside reconnection rate starts to intensify before the substorm onset, but a detailed analysis must be carried out to discriminate between the
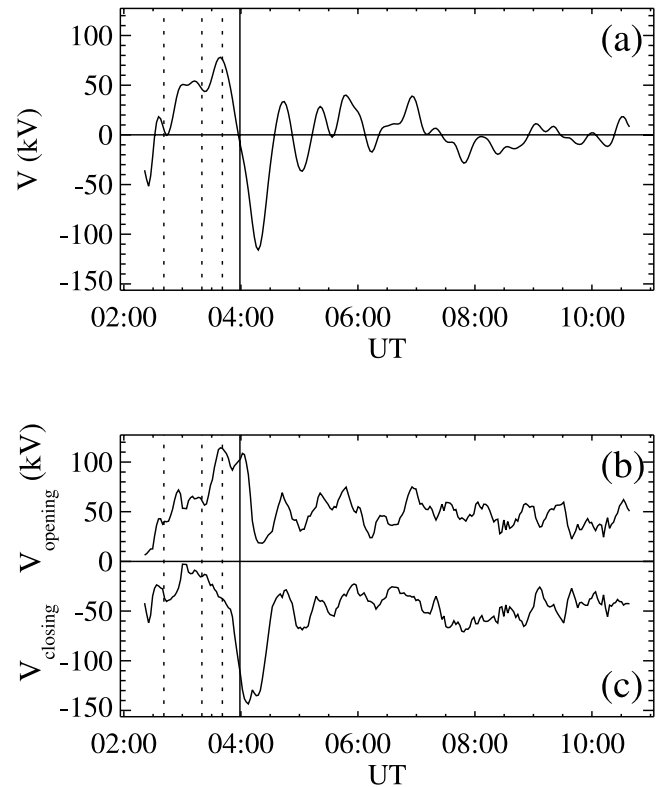
**Figure 12.** (a) Open magnetic flux (raw and smoothed values) threading the northern polar cap versus time, deduced from IMAGE FUV SI12 data on 29 December 2000. (b) Time derivative of the smoothed open magnetic flux shown in Figure 12a. Shaded areas indicate periods of southward IMF from the Wind data shown in Figure 13. Vertical solid lines indicate the times of substorm onsets, while dashed lines indicate pseudobreakups



**Figure 14.** (a) Difference between dayside and nightside reconnection voltages for the interval on 29 December 2000, equal to the rate of change of open flux; (b) dayside reconnection voltage (i.e., open flux production rate); and (c) nightside reconnection voltage (i.e., open flux closure rate), obtained using the boundary motion deduced from SI12 images and the convection electric field deduced from SuperDARN data. Vertical solid lines indicate the times of substorm onsets, while dashed lines indicate pseudobreakups.



**Figure 13.** IMF (GSM) components from Wind spacecraft measurements on 29 December 2000. During this interval, the Wind spacecraft was located at GSE coordinates $(X, Y, Z) \approx (6, 250, 17)$ $R_E$.

effect of smoothing and a possible real timing difference. Two pseudobreakups took place during the period preceding the onset at 0359 UT, as in fact often occurs during the growth phase. The computed nightside reconnection rate drops to nearly zero at 0304 UT, about an hour before the substorm onset and 16 min prior to the pseudobreakup at 0320 UT. During this hour, the computed nightside reconnection rate progressively intensifies, more steeply during the ten minutes preceding the onset. We consider that this increase leading up to the onset is real (significantly longer than ~16 min), resulting in the observed pseudobreakups. However, we cannot determine whether the nightside flux closure increases progressively, or if it suddenly increased at the time of the observed pseudo-breakups. It must be noted that the GOES 8 satellite, ideally located near the midnight sector at the time of the pseudobreakups and onset, recorded a variation of the $B_x$ component of the magnetospheric field suggesting a dipolarization (not shown). Also the $AE$ and $AL$ indices were disturbed prior to what we identify as the onset. Examination of magnetograms from the CANOPUS-CARISMA and IMAGE (for International Monitor for Auroral Geomagnetic Effects, not to be confused with the IMAGE satellite) networks (not shown) would rather indicate that the brightening recorded at 0341 can be considered as an intense pseudobreakup, despite similarities with substorm onsets. Indeed, the spot of the pseudobreakup is still bright at the time of the onset thus mixing both signatures. This suggests that both features could be intimately linked together, so that the possibility of a multiple onset scenario cannot be categorically ruled out. Nevertheless, the thickening of the oval characteristic of an expansion phase is observed following the brightening of 0359 UT, and the open flux keeps increasing until that time, indicating that the end of the growth phase is taking place. This leads us to the conclusion that the substorm onset is actually the brightening observed at 0359 UT. Several authors [Aikio et al., 1999; Akasofu, 1964; Koskinen et al., 1993] considered that pseudobreakups and substorm onsets are not of fundamentally different physical nature, and only differ in magnitude and in the conditions met at the time of their development. From that standpoint, we can expect to record disturbances with ground-based magnetometers in response to a pseudobreakup, revealing a modification of the current systems, and it seems natural as well to find that both pseudobreakups and substorms are associated with flux closure. Along the same lines, a dipolarization cannot be ruled out during a pseudobreakup, since it is a natural signature of magnetic reconnection in the tail. The computed nightside reconnection rate reaches its maximum magnitude (140 kV) about ten minutes after onset and then returns to quiet values varying around ~40 kV. The maximum rate of flux closure is obtained roughly at the time of the onset or shortly after. This extreme value could be as high as ~160 kV, taking the smoothing into account. The onset of the substorm presented in this section was preceded by an interval of intense dayside reconnection (between 120 and 130 kV, Figure 14b) feeding the magnetosphere with open magnetic flux. This interval of intense flux opening sets up the necessary conditions to produce the development of a substorm (i.e., accumulation of open flux) and is thus the growth phase of the substorm considered,
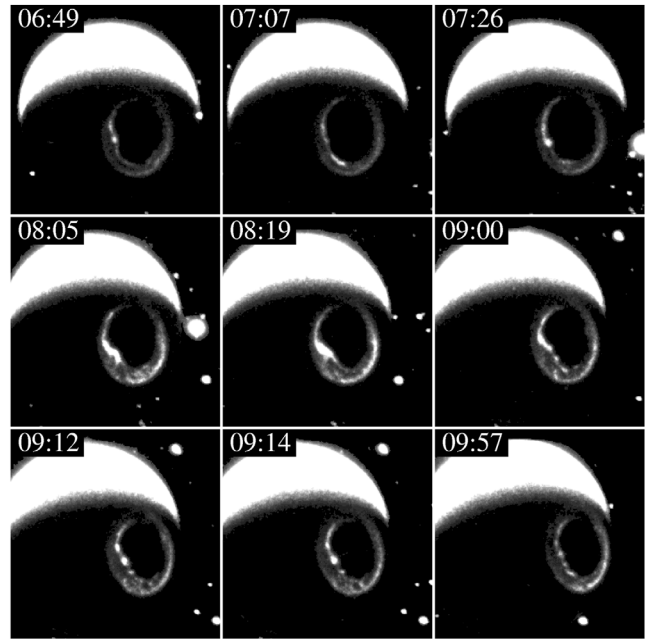


**Figure 15.** FUV-WIC images obtained between 0630 and 1000 UT. The dayglow appears at the top of each frame. The PBI appears as the bright structure at the inner edge of the auroral oval.

despite the absence of a switch in sense of IMF $B_z$. Figure 15 presents WIC images obtained after 06:30 UT, which show the PBI at different times between 0630 and 1000 UT. Note that the oscillations present in the nightside voltage prior to 0600 UT appear to be driven by a roughly periodic variation of the dayside reconnection voltage (with some phase displacement between these two curves, as naturally expected). The nightside reconnection voltage progressively increases after 0630 UT, and finally dominates the dayside flux opening voltage leading to a global contraction of the polar cap. This increase of the flux closure rate reaches 68 kV and departs from the sudden intensification of the nightside voltage associated with an expansion phase onset. A brightening of the PBI is also seen, and the morphology of the oval evolves to a shape similar to expansion phase conditions (Figure 15 after 0800 UT). This interval suggests that an intensification of the flux closure rate of the magnetosphere can activate the auroral precipitation in the PBI, and thus suggests a direct relation between PBI auroral structures and flux closure in the magnetotail.

[30] Finally, we calculated the characteristic solar wind-scale length for reconnection L using both method 1 (not shown), and method 2 (Figure 16) discussed previously. As the IMF was always southward during the interval considered, the transfer function is always quite large (Figure 16a), and the dayside voltage is also nearly always high (Figure 16b). It should be noted that the dayside voltage reached a maximum value of 130 kV around 0340 UT, roughly at the time the transfer function reached a local minimum, indicating that care must be taken when using a transfer function to evaluate the dayside voltage. At this time, we obtain L ~ 18 $R_E$. The characteristic solar wind-scale length calculated here indicates strong temporal
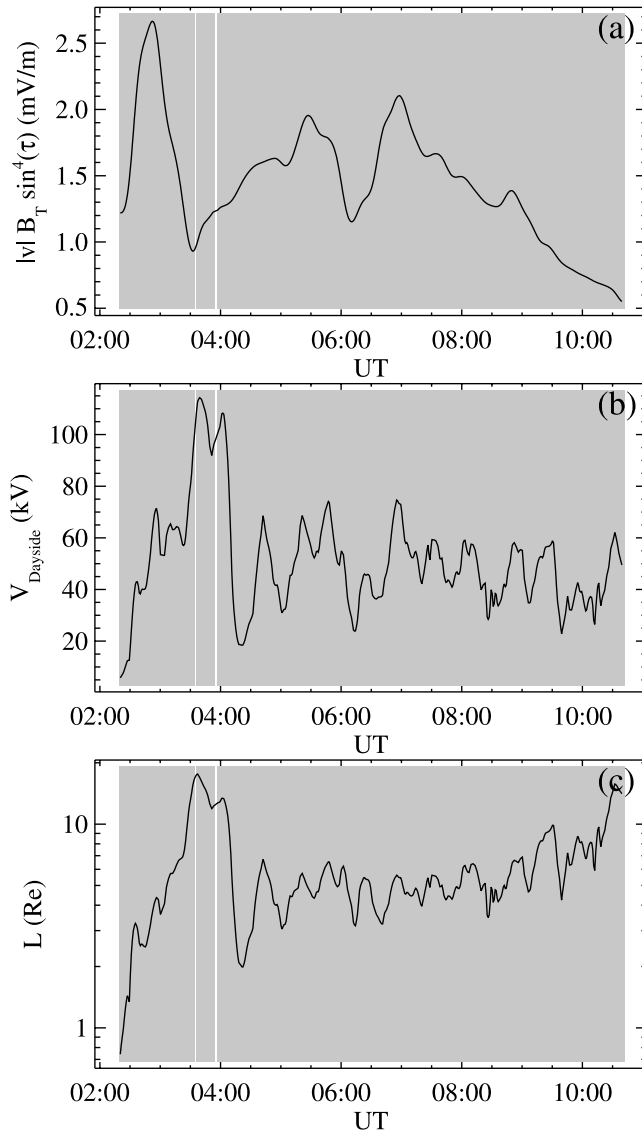
**Figure 16.** (a) Transfer function given by equation (7) calculated from the Wind solar wind data on 29 December 2000, (b) dayside reconnection rate computed using SI12 and SuperDARN data, and (c) solar wind reconnection scale width L calculated from the ratio of Figures 16a and 16b). Shaded areas indicate intervals of southward IMF.

variability, but remains of a reasonable order of magnitude. These values can be compared with a length obtained with method 1 of ~8 $R_E$ between 0220 and 0310 UT, and ~3 $R_E$ between 0310 and 1040 UT.

### 4.3. Other Cases

[31] We studied four other time intervals of ~9 h each close to winter solstice 2000 (0335 to 1215 UT on 23 December, 1800 UT on 23 December to 0315 UT on 24 December, 1215 to 2225 UT on 25 December, and 0300 to 1200 UT on 26 December), and reached similar conclusions. Flux closure can take place prior to substorm onset resulting in pseudobreakups during the growth phase. Maximum flux closure is generally reached roughly at the

time of the substorm onset. The flux closure rate slowly decreases (in absolute value) after the onset, back to ~30 to ~40 kV. However, some substorms were found to depart from this simple picture, especially during periods of prolonged intense nightside reconnection rates (such as 23 and 24 December 2000 for example), making the substorm analysis more complicated, especially the optical identification of the substorm onset. The maximum rate of flux closure is then variable, but generally above 100 kV.

## 5.  Discussion

[32] Several sources of uncertainties can complicate the calculation of the amount of open flux and the reconnection rates determined by combining IMAGE FUV SI12 images of the proton aurora and SuperDARN measurements of the convection flow. The first source is the temporal smoothing that must be applied when determining the velocity of the open/closed field line boundary. As already discussed in the preceding sections, this smoothing results in a smearing of short-timescale features. As a result, the increase in the computed nightside reconnection rate is seen ~12 to 14 min prior to onset, and a temporal difference less than ~16 min is probably not significant. However, when substorm onsets are preceded by pseudobreakups, some significant flux closure is found prior to onset though its detailed time dependence (a transient or more gradual variation) cannot be determined. A second side effect of the smoothing is an underestimate (in absolute value) of the maximum nightside voltage.

[33] A second source of uncertainty lies in the least squares fit used to represent the open/closed boundary with a Fourier series. This fitted series cannot always reproduce the details of the boundary. On the other hand, it spatially smooths the boundary determined from the SI12 images. The fitted Fourier series is smooth in essence and filters out the noise around the boundary. However, on some occasions, this fitted boundary departs locally from the actual boundary because of the oscillation of the terms in the Fourier series. The temporal smoothing partly corrects for this drawback by averaging these unrealistic oscillations. In addition, the Fourier series can be extrapolated when a part of the proton oval is not bright enough to be detected using SI12.

[34] We also note that our identification of the open/closed field boundary does not include a particular treatment of the cusp. As a bright feature, the cusp is not distinguished from the auroral oval. However, the cusp is threaded by open field lines whereas the auroral oval is threaded by closed field lines. This leads to an underestimate of the open magnetic flux by a few percent, which is not likely to be of major significance. The effect on the computed voltages has already been discussed in section 3.

[35] Another source of error is associated with the electric field determined using the SuperDARN data. The location of the SuperDARN radars does not allow a complete coverage of the northern region. Consequently, when the electric potential is determined using a least squares fit (constrained by a model), it generally includes some extrapolation, which can sometimes depart from the actual potential. In addition, the appearance or disappearance of radar echoes in the polar cap can occur abruptly, modifying

the fitted electric field. This can lead to artificial variations of the reconnection voltages determined. Nevertheless, the smoothing versus time that is applied should reduce the effect of transient unrealistic variations on the computed voltages. However, the bulk of the total electric field results from the motion of the open/closed boundary, especially during substorms, or in other words the boundary moves first and some time later convection gradually redistributes the flux to an equilibrium position [*Cowley and Lockwood*, 1992].

[36] One can also question the relation between the electric field and voltage computed in the ionosphere and the electric field and voltage at the reconnection site: some potential drop might take place between the ionosphere and the reconnection site. It is however often assumed as a first approximation that magnetic field lines are electric equipotentials, because the conductivity is much larger in the direction parallel to the magnetic field than in the perpendicular direction. This assumption may be erroneous in the presence of strong field aligned currents. A detailed treatment of this potential drop requires additional data, and would ideally lead to a complete 3-D reconstruction of the electric potential.

[37] As already discussed in section 3, we can unambiguously identify flux closure prior to substorm expansion onset only if the timescale involved is larger than ~16 min. Nevertheless, we showed that flux closure does take place prior to onset, associated with pseudobreakups. The natural question is then what makes the difference between a pseudobreakup and an expansion onset? The total amount of open flux present does not seem to be a key factor, in the sense that an onset of flux closure can apparently evolve into either a substorm expansion or a pseudobreakup at a given value of open flux. On the other hand, the magnitude of the rate of flux closure is much larger at substorm onset than for a pseudobreakup. This suggests some difference in the mechanism responsible for the auroral particle precipitation, either concerning the physical process responsible for the flux closure or the control parameters governing this process, such as the size of the reconnection site, or the magnitude of the electric field at the reconnection site, for example. (We note that the pseudobreakups discussed here all take place during the growth phase and may differ from other pseudobreakups, such as the recovery phase pseudobreakups discussed by *Kullen and Karlsson* [2004]). In a similar way, several parameters can control the maximum magnitude of the nightside flux closure voltage at substorm onset. One would indeed expect that the rate of flux closure should be bounded by some physical constraints on the detailed mechanism responsible for the magnetic field line reconnection, including, for example, the maximum possible size of the neutral line along which the closure takes place, the magnitude of the electric field, the degree of field line stretching, the plasma density and conductivity, the energy density, etc. Although a preliminary statistical survey of flux closure during substorms has been conducted [*Milan et al.*, 2006], a much broader study is required. Our technique will form the basis of such a study. From a magnetospheric standpoint, a maximum flux closure reached shortly after onset is consistent with the near earth neutral line

mechanism. However, cases were found that depart from that strict time dependence, suggesting that other mechanisms can possibly coexist.

## 6.  Conclusions and Perspectives

[38]  In this paper, we have proposed a systematic method to determine the open magnetic flux, and the dayside and nightside reconnection rates separately, using IMAGE FUV SI12 and SuperDARN data. This method involves (1) determination of the open/closed field line boundary and its motion using the SI12 images, (2) determination of the convection electric field along the boundary using SuperDARN data, and (3) application of Faraday's law. We find that the reconnection rates can be computed with a temporal resolution of about 15 min. Applying the method to substorms, we find that the nightside flux closure is generally maximum at the time of the onset, and that it can start intensifying prior to onset, resulting in pseudobreakups. After the onset, the nightside voltage slowly returns to values typical of quiet periods, that is, between ~30 and ~40 kV. The nightside voltage at substorm onset is generally above 100 kV, whereas the voltage at the time of the pseudobreakup is significantly smaller in magnitude. Further studies will be undertaken to determine what parameters control the magnitude of the nightside flux closure at substorm onset and during the pseudobreakups which occasionally precede them.

[40]  Arthur Richmond thanks Lyons Larry and J. Ruohoniemi for their assistance in evaluating this paper.

## References

Aikio, A. T., V. A. Sergeev, M. A. Shukhtina, L. I. Vagina, V. Angelopoulos, and G. D. Reeves (1999), Characteristics of pseudobreakups and substorms observed in the ionosphere, at the geosynchronous orbit, and in the midtail, *J. Geophys. Res.*, *104*(A6), 12,263.

Akasofu, S.-I. (1964), The development of the auroral substorm, *Planet. Space Sci.*, *12*, 273.

Baker, J. B., C. R. Clauer, A. J. Ridley, V. O. Papitashvili, M. J. Brittnacher, and P. T. Newell (2000), The nightside poleward boundary of the auroral oval as seen by DMSP and the Ultraviolet Imager, *J. Geophys. Res.*, *105*, 21,267.

Blanchard, G. T., L. R. Lyons, J. C. Samson, and F. J. Rich (1995), Locating the polar cap boundary from observations of 6300 Å auroral emission, *J. Geophys. Res.*, *100*, 7855.

Blanchard, G. T., L. R. Lyons, O. de la Beaujardière, R. A. Doe, and M. Mendillo (1996), Measurement of the magnetotail reconnection rate, *J. Geophys. Res.*, *101*, 15,265.

Blanchard, G. T., L. R. Lyons, and J. T. Samson (1997a), Accuracy of using the 6300 Å auroral emission to identify the magnetic separatrix on the nightside of the Earth, *J. Geophys. Res.*, *102*, 9697.

Blanchard, G. T., L. R. Lyons, and O. de la Beaujardière (1997b), Magneto-tail reconnection rate during magnetospheric substorms, *J. Geophys. Res.*, *102*, 24,303.

Chisham, G., M. P. Freeman, I. J. Coleman, M. Pinnock, M. R. Hairston, M. Lester, and G. Sofko (2004), Measuring the dayside reconnection rate during an interval of due northward interplanetary magnetic field, *Ann. Geophys.*, *22*, 4243.

Chisham, G., M. P. Freeman, T. Sotirelis, R. A. Greenwald, M. Lester, and J.-P. Villain (2005), A statistical comparison of SuperDARN spectral width boundaries and DMSP particle precipitation boundaries in the mourning sector ionosphere, *Ann. Geophys.*, *23*, 733.

Cowley, S. W. H., and M. Lockwood (1992), Excitation and decay of solar wind-driven flows in the magnetosphere-ionosphere system, *Ann. Geophys.*, *10*, 103.

Dungey, J. W. (1961), Interplanetary field and the auroral zones, *Phys. Res. Lett.*, *6*, 47.

Feldman, W. C., et al. (1984), Evidence for slow mode shocks in the distant geomagnetic tail, *Geophys. Res. Lett.*, *11*, 599.

Feldman, W. C., R. L. Tokar, J. Brin, E. W. Hones Jr., S. J. Bame, and C. T. Russel (1987), Structure of a slow mode shock observed in the plasma sheet boundary layer, *J. Geophys. Res.*, *92*, 83.

Gérard, J.-C., B. Hubert, A. Grard, M. Meurant, and S. B. Mende (2004), Solar wind control of auroral substorm onset locations observed with the IMAGE-FUV imagers, *J. Geophys. Res.*, *109*, A03208, doi:10.1029/2003JA010129.

Grocott, A., S. W. H. Cowley, J. B. Sigwarth, J. F. Watermann, and T. K. Yeoman (2002), Excitation of twin-vortex flow in the nightside high-latitude ionosphere during an isolated substorm, *Ann. Geophys.*, *20*, 1577.

Ho, C. M., B. T. Tsurutani, E. J. Smith, and W. C. Feldman (1994), A detailed examination of an X-line region in the distant tail: ISEE-3 observations of jet flow and Bz reversals and pair of slow shocks, *Geophys. Res. Lett.*, *21*, 3031.

Koskinen, H. E. J., R. E. Lopez, R. J. Pellinen, T. J. Pulkkinen, D. N. Baker, and T. Bosinger (1993), Pseudobreakup and substorm growth phase in the ionosphere and magnetosphere, *J. Geophys. Res.*, *98*, 5801.

Kullen, A., and T. Karlsson (2004), On the relation between solar wind, pseudobreakups, and substorms, *J. Geophys. Res.*, *109*, A12218, doi:10.1029/2004JA010488.

Liou, K., P. T. Newell, C. I. Meng, M. Brittnacher, and G. Parks (1998), Characteristics of solar wind controlled auroral emissions, *J. Geophys. Res.*, *103*, 17,543.

Lyons, L. R., E. Zesta, Y. Xu, E. R. Sánchez, J. C. Samson, G. D. Reeves, J. M. Ruohoniemi, and J. B. Sigwarth (2002), Auroral pole-ward boundary intensifications and tail bursty flows: A manifestation of a large-scale ULF oscillation?, *J. Geophys. Res.*, *107*(A11), 1352, doi:10.1029/2001JA000242.

Mende, S. B., et al. (2000a), Far ultraviolet imaging from the IMAGE spacecraft: 1. System design, *Space Sci. Rev.*, *91*, 243.

Mende, S. B., et al. (2000b), Far ultraviolet imaging from the IMAGE spacecraft: 3. Spectral imaging of Lyman alpha and OI 135.6 nm, *Space Sci. Rev.*, *91*, 287.

Milan, S. E. (2004), A simple model of the flux content of the distant magnetotail, *J. Geophys. Res.*, *109*, A07210, doi:10.1029/2004JA010397.

Milan, S. E., M. Lester, S. W. H. Cowley, K. Oksavik, M. Brittnacher, R. A. Greenwald, G. Sofko, and J.-P. Villain (2003), Variations in the polar cap area during two substorm cycles, *Ann. Geophys.*, *21*, 1121.

Milan, S. E., S. W. H. Cowley, M. Lester, D. M. Wright, J. A. Slavin, M. Fillingim, C. W. Carlson, and H. J. Singer (2004), Response of the magnetotail to changes in the open flux content of the magnetosphere, *J. Geophys. Res.*, *109*, A04220, doi:10.1029/2003JA010350.

Milan, S. E., J. A. Wild, A. Grocott, and N. C. Draper (2006), Space- and ground-based investigations of solar wind-magnetosphere-ionosphere coupling, *Adv. Space. Res*, in press.

Newell, P. T., S. Wing, C. I. Meng, and V. Sigillito (1991), The auroral oval position, structure and intensity of precipitation from 1984 onward: An automated on-line data base, *J. Geophys. Res.*, *96*, 5877.

Østgaard, N., J. Moen, S. B. Mende, H. U. Frey, T. J. Immel, P. Gallop, K. Oksavik, and M. Fujimoto (2005), Estimates of magnetospheric reconnection rate based on IMAGE-FUV and EISCAT measurements, *Ann. Geophys.*, *23*, 123.

Ruohoniemi, J. M., and K. B. Baker (1998), Large-scale imaging of high-latitude convection with Super Dual Auroral Radar Network HF radar observations, *J. Geophys. Res.*, *103*, 20,797.

Ruohoniemi, J. M., and R. A. Greenwald (1996), Statistical patterns of high-latitude convection obtained from Goose Bay HF radar observations, *J. Geophys. Res.*, *101*, 21,743.

Sergeev, V. A., E. M. Sazhina, N. A. Tsyganenko, J. Å. Lundblad, and F. Søraas (1983), Pitch-angle scattering of energetic protons in the magnetotail current sheet as the dominant source of their isotropic precipitation into the nightside ionosphere, *Planet. Space Sci.*, *31*, 1147.

Siscoe, G. L., and T. S. Huang (1985), Polar cap inflation and deflation, *J. Geophys. Res.*, *90*, 543.

Smith, E. J., J. A. Slavin, B. T. Tsurutani, W. C. Feldman, and S. J. Bame (1984), Slow mode shocks in the Earth's magnetotail: ISEE-3, *Geophys. Res. Lett.*, *11*, 1054.

Vasyliunas, V. M. (1984), Steady state aspects of magnetic field line merging, in *Magnetic Reconnection in Space and Laboratory Plasmas*, *Geophys. Monogr. Ser.*, vol. 30, edited by E. W. Hones Jr., pp. 25–31, AGU, Washington, D. C.

Wygant, J. R., R. B. Torbert, and F. S. Mozer (1983), Comparison of S3-3 polar cap potential drops with the interplanetary magnetic field and models of the magnetopause reconnection, *J. Geophys. Res.*, *88*, 5727.

————————————

C. Blockx, J.-C. Gérard, and B. Hubert, Laboratoire de Physique Atmosphérique et Planétaire, University of Liège, Allée du 6 Août, 17, Bat B5c, Liège B-4000, Belgium. (b.hubert@ulg.ac.be)

S. W. H. Cowley, A. Grocott, and S. E. Milan, Department of Physics and Astronomy, University of Leicester, Leicester LE1 7RH, UK.